Journal of Nuclear Medicine & Radiation Therapy

Schreiter et al., J Nucl Med Radiat Ther 2016, 7:5
DOI: 10.4172/2155-9619.1000302

Research Article Open Access

Comparison of [^{68}Ga]Ga-PSMA-HBED-CC PET versus Whole-Body Bone Scintigraphy for the Detection of Bone Metastases in Patients with Prostate Cancer

Vera Schreiter*, Maximilian Gericke, Uwe Heimann, Ingo Steffen, Lars Stelter, Martin H. Maurer, Bernd Hamm, Winfried Brenner, Dorothea Theilig, Johannes Kahn and Nils Friedemann Schreiter

Department of Radiology, Charité-Universitätsmedizin Berlin, Berlin, Germany

***Corresponding author:** Vera Schreiter, Department of Radiology, Charité-Universitätsmedizin, Augustenburger Platz 1, 13353 Berlin, Germany, Tel: +49 30-450657165; Fax: +49-30- 450 557989; E-mail: vera.schreiter@charite.de

Received date: July 20, 2016; **Accepted date:** August 09, 2016; **Published date:** August 16, 2016

Abstract

Aim: To compare [^{68}Ga]Ga-PSMA-HBED-CC PET and (^{99}m)Tc-DPD bone scintigraphy for the detection of bone metastases from prostate cancer.

Methods: [^{68}Ga]Ga-PSMA-HBED-CC PET/CT and (^{99}m)Tc-DPD bone scintigraphy in 19 men with histopathological proven prostate cancer were compared to each other for the sensitivity/specificity, accuracy, positive predictive value (PPV) and negative predictive value (NPV) for the detection of bone metastases.

Results: According to the standard of reference lesion-based analysis of [^{68}Ga]Ga-PSMA-HBED-CC PET and (^{99}m)Tc-DPD bone scintigraphy reached a sensitivity of 45.6%/34%, specificity of 86.4%/81.4%, accuracy of 60.5%/51.2%, positive predictive value of 85.5%/76.1%, and negative predictive value of 47.7%/41.4%, respectively.

Conclusion: [^{68}Ga]Ga-PSMA-HBED-CC PET could detect significantly more bone metastases in prostate cancer than (^{99}m)Tc-DPD bone scintigraphy.

Keywords: [^{68}Ga]Ga HBED-CC PSMA; (^{99}m)Tc-DPD scintigraphy; Bone metastases; Detection rate; Prostate cancer

Abbreviations: PPV: Positive Predictive Value; NPV: Negative Predictive Value; PSMA: Prostate Specific Membrane Antigen; ^{18}F-choline: ^{18}F-fluoromethylcholine; PET/CT: Positron Emission Tomography/Computed Tomography; LEHR: Low-Energy High-Resolution Collimator; BS: Bone Scan; PSA: Prostate Specific Antigen; SD: Standard Deviation; HU: Hounsfield Units; RRP: Radical Retropubic Prostatectomy; LNE: Lymphadenoctomy; RTX: Radiotherapy; AHT: Anti-Hormonal Treatment

Introduction

^{68}Ga-labeled Glu-urea-Lys(Ahx)-HBED-CC ([^{68}Ga]Ga HBED-CC PSMA) has recently emerged as a new radiotracer. It is a promising candidate for staging and re-staging prostate cancer using hybrid imaging technology such as positron emission tomography/computed tomography (PET/CT) [1-3]. Prostate-specific membrane antigen (PSMA) is expressed by almost all prostate cancer cells and is used as a target for imaging and therapy [4-6].

Imaging with [^{68}Ga]Ga-PSMA-HBED-CC has shown advantages over ^{18}F-fluoromethylcholine (^{18}F-choline) PET/CT - the molecular imaging modality currently used in patients with suspected recurrence of prostate cancer based on laboratory chemistry tests: [^{68}Ga]Ga-PSMA-HBED-CC PET/CT improves detection of prostate cancer and its metastases due to higher specific radiotracer uptake rates within the abnormal lesions and lower tracer uptake in surrounding normal tissue. Detection is especially improved in patients with small increases in prostate-specific antigen (PSA) levels [7]. In contrast, the value of [^{68}Ga]Ga-PSMA-HBED-CC PET/CT vis a vis technetium-99m-3,3-diphosphono-1,2-propanedicarboxylic acid ((^{99}m)Tc-DPD) bone scintigraphy (BS) remains to be determined. The latter is currently used for detection of bone metastases in patients with high-risk prostate cancer. Prostate cancer is the most common cancer of men in western industrialized countries [8]. In 2012 alone, there were 28,000 prostate cancer deaths in the United States [9]. Prostate cancer tends to metastasize to the skeletal system [10]. Most skeletal prostate cancer metastases are osteoblastic, but other types of bone metastases, such as osteolytic or mixed types, can also occur [11].

BS with (^{99}m)Tc-DPD detects the pathological osteoblastic response adjacent to metastatic bone lesions, making it a highly sensitive and cost-efficient whole body staging modality for bone metastases associated with prostate cancer [12]. The aim of this study was to compare the sensitivity, specificity, accuracy, and the positive/negative predictive value (PPV/NPV) of [^{68}Ga]Ga-PSMA-HBED-CC PET and (^{99}m)Tc-DPD BS in the detection of different types of bone metastases in prostate cancer patients.

Material and Methods

Patients

We performed a database search for patients with prostate cancer who underwent standardized [^{68}Ga]Ga-PSMA-HBED-CC (^{68}Ga-DKFZ-11) PET/CT and (^{99}m)Tc-DPD (Teceos®, CIS bio GmbH, IBA

Molecular, Germany) BS for prostate cancer staging at our institution. The [^{68}Ga]Ga-PSMA-HBED-CC PET/CT was done as additional imaging modality depending on the patients risk of having metastases or after unclear findings in former imaging. Inclusion criteria were: PET/CT and BS performed no more than one month apart; both examinations performed according to the institutional standard protocols; no relevant changes in tumor surrogate parameters, no relevant clinical deterioration, and no cancer-specific treatment of patients between the two imaging examinations. Following these criteria we included 19 patients in our analysis.

The clinical data documented for each patient included histopathologically proven prostate cancer if available, Gleason score evaluation, PSA levels, and clinical stage at time of prostate cancer diagnosis as well as prior imaging by [^{68}Ga]Ga-PSMA-HBED-CC PET/CT and (^{99}m)Tc-DPD BS. Clinical parameters were used to categorize cancer into low, medium and high-risk. Clinical data were retrieved from the patients' digital hospital files and by telephone interview, if needed.

All reported investigations were conducted in accordance with the Helsinki declaration and with our national regulations. The institutional review board approved this retrospective study under the number EA1/354/14. All patients gave written informed consent and agreed to evaluation and publication of their anonymized data.

(^{99}m)Tc-DPD BS

Planar (^{99}m)Tc-DPD BS was performed 1 h and 2.5 h to 3 h after intravenous (IV) injection of approx. 700 Megabecquerel (MBq) (^{99}m)Tc-DPD. Planar images were acquired using a hybrid dual-head Siemens Symbia TruePoint T6 SPECT/CT system (Siemens Medical Solutions, Erlangen, Germany) with a scan speed of 10 cm/min and a 256 × 1024 matrix. When diagnostic confidence in interpreting planar scans was poor, an additional SPECT/CT scan was obtained.

Technical parameters for the gamma camera were as follows: crystal thickness of 9.5 mm, 53.3 cm axial by 38.7 cm diameter SPECT field of view (FOV) and 6-slice CT scanner. Acquisition was performed in a 128 × 128 matrix, zoom 1.0, pixel size of 4.8 mm, and non-circular orbit (auto contour) with 30 projections over 180° (continuous acquisition). A low-energy high-resolution collimator (LEHR) was used with dual-energy windowing and a lower scatter energy window (15% width) for scatter estimation.

[^{68}Ga]Ga-PSMA-HBED-CC PET/CT

PET/CT was performed with [^{68}Ga]Ga-PSMA-HBED-CC (=^{68}Ga-DKFZ-PSMA-11). Tracer synthesis is described in detail in [4]. The PET scan was initiated approx. 1 h after IV injection of approx. 120 MBq [^{68}Ga]Ga-PSMA-HBED-CC. Ten to twelve bed positions with 90 sec per position were scanned with a 144 × 144 acquisition matrix and 576 mm FOV. The whole-body CT examination was performed immediately before the PET acquisition was started. Generally, the whole-body scan was performed from mid-thigh to the skull base.

The CT scan included in the PET/CT examination was acquired without contrast medium or, if indicated for whole-body staging, with 80 ml to 120 ml of Ultravist 370 (Bayer HealthCare Pharmaceuticals, Berlin, Germany) injected as a bolus at a rate of 2-3 ml/s. A venous contrast phase (70 sec after contrast agent administration) was acquired with 16 mm × 1.5 mm reconstructed slice thickness and used for attenuation correction of the PET dataset. CT examinations were performed on a Philips Gemini TF ToF 16 scanner (Philips Medical Systems, Cleveland, USA) using the following technical parameters: 120 kV; 100 mAs to 250 mAs with dose modulation (D-DOM).

Image reading

One physician of nuclear medicine and radiology (>9 years of experience) and one radiologist specialized in hybrid imaging (>5 years of experience) assessed whole-body CT scans for the presence of bone metastases in consensus. All bone metastases were classified morphologically into osteoblastic, osteolytic, or mixed types as well as in terms of their localization using the CT data.

Attenuation-corrected [^{68}Ga] PSMA HBED-CC PET images and planar (^{99}m)Tc-DPD BS were interpreted for the presence of bone metastases with the readers blinded to the results of CT and other imaging modalities. Only lesions evaluable in all imaging modalities were interpreted.

Criteria for bone metastasis in PET and BS were a pathological SUV max and lesions in the CT were rated by their morphology. When tracer uptake was inconclusive in terms of lesion characterization, the readers additionally used CT and SPECT/CT datasets for assessment. Size of bone metastases and Hounsfield units (HU) were measured by one observer using the CT data. CT and clinical parameters as described above served as standard of references.

Statistical analysis

Demographic data are given as mean, range and standard deviation (SD). Lesion-based results were compared for PET and BS using the McNemar test. Patient-based results were compared using the two-sided Fisher's exact test for unpaired samples. Statistical significance was accepted at $p<0.05$. Statistical analysis was performed using the SPSS software package (SPSS 20.0.0.; SPSS Corporation, Chicago, USA).

Results

Nineteen patients (mean age: 62.3 years, range: 53.5-76.1) with histologically proven prostate cancer met our criteria and were included in the analysis. Most patients underwent prostatectomy, some with additional lymphadenectomy and/or additional local radiotherapy. Table 1 summarizes the treatment histories of all patients prior to [^{68}Ga]Ga-PSMA-HBED-CC PET/CT and (^{99}m)Tc-DPD BS.

All patients with histopathological examination had medium- to high-risk prostate cancer, except one patient with low-risk prostate cancer, with a mean Gleason score of 8.1 (median 8.0; range: 6-10). The mean initial PSA level at diagnosis was 27.2 ng/ml ± 24.4 SD (range: 3.4 ng/ml to 80 ng/ml). Mean PSA level prior imaging by [^{68}Ga]Ga-PSMA-HBED-CC PET/CT and (^{99}m)Tc-DPD BS was 13.8 ng/ml ± 20.3 SD (range: 0.5 ng/ml to 60 ng/ml). The CT scans revealed a total of 162 bone lesions. Fifty-eight lesions were rated as benign bone lesions (e.g. osteoids) and 104 lesions were classified as bone metastases.

Of the latter, 93.3% (n=97) were classified as osteoblastic, 4.6% (n=5) as osteolytic, and 1.9% (n=2) as mixed metastases (Figure 1). Applying PET scans, 47 lesions were rated as malignant as compared to 35 lesions in BS. Compared to the CT findings, PET had a sensitivity of 45.6%, specificity of 86.4%, accuracy of 60.5%, PPV of 85.5%, and NPV of 47.7% for the detection of bone metastases (Figure 2).

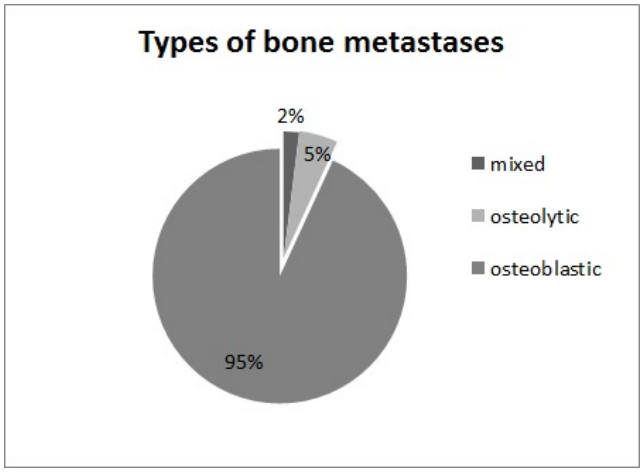

Figure 1: Types of bone metastases.

BS with (^{99}m)Tc-DPD had 34% sensitivity, 81.4% specificity, 51.2% accuracy, PPV of 76.1%, and NPV of 41.4%, compared to CT (Figure 2). A subtype analysis of morphologic types of bone metastases for each imaging modality was not performed due to the uneven distribution of lesion types.

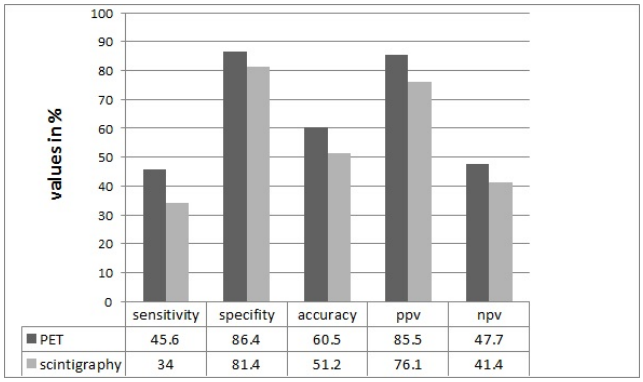

	sensitivity	specifity	accuracy	ppv	npv
PET	45.6	86.4	60.5	85.5	47.7
scintigraphy	34	81.4	51.2	76.1	41.4

Figure 2: Results of PET (dark grey cases) and Bone Scintigraphy (light grey cases) in comparison to CT.

Sensitivity for the detection of bone metastases was significantly higher for [^{68}Ga]Ga-PSMA-HBED-CC PET than for (^{99}m)Tc-DPD BS ($p<0.002$), while specificity was not significantly different. A total of 49 bone metastases in 4 patients were false-negative based on [^{68}Ga]Ga-PSMA-HBED-CC PET versus 58 metastases in 6 patients based on (^{99}m)Tc-DPD BS. All false-negative bone metastases were classified as osteoblastic metastases with small diameter (<10 mm) and high attenuation (670 HU to 1052 HU) in CT. On a per patient-analysis of sensitivity and specificity of PET and BS compared to CT-findings, we found a sensitivity of 92% and specificity of 83% for PET, respective 82% and 83% for BS. Patient-based analysis of false-negative bone metastases using the two-sided Fisher's exact test revealed a trend towards a lower rate of false-negative radiotracer uptake rates in [^{68}Ga]Ga-PSMA-HBED-CC PET compared to (^{99}m)Tc-DPD BS ($p=0.013$). All patients with false-negative bone metastases in PET and/or BS had a history of systemic treatment. Overall, 9 patients of the study population underwent systemic treatment prior to imaging (antihormone therapy, chemotherapy, etc.) (Table 1). Patient-based analysis of the potential gain in diagnostic information achieved with either PET or BS showed the following results: 13 true-positive bone metastases in 6 patients detected by PET (Figure 3) compared to one additional lesion detected by BS. Conversely, (^{99}m)Tc-DPD BS had a diagnostic gain of one lesion in one patient compared with PET (Figure 4). In this case, the lesion in the 10th rib was missed by PET imaging because abnormal tracer uptake of the lesion was obscured by normal tracer uptake in the liver. After [^{68}Ga]Ga-PSMA-HBED-CC PET the therapeutic approach was changed in 58% (11/19) patients. Of these, 6 (54.5%) received additional systemic treatment, 4 (36.4%) had a RT of bone metastases and 1 (9.1%) was treated by a combination AHT and RT of the bone (Table 1). In [^{68}Ga]Ga-PSMA-HBED-CC PET/CT there were found additionally 4 primary prostatic lesions in 4 patients and 19 lymph node metastases in 7 patients. There were no distant visceral metastases in any imaging modality.

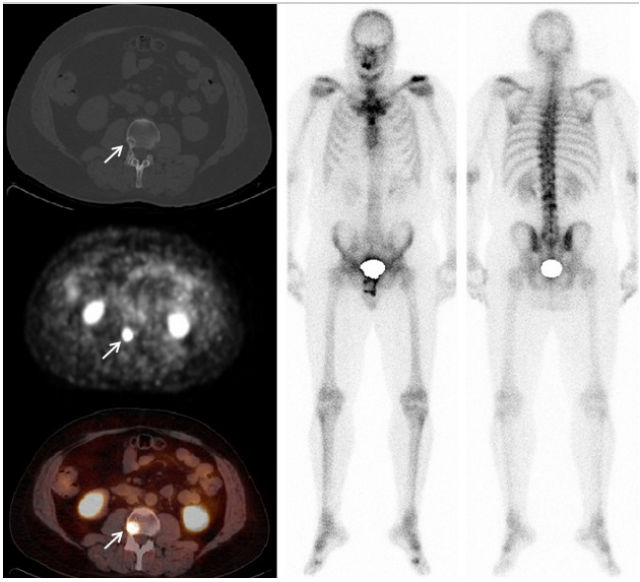

Figure 3: [^{68}Ga]Ga-PSMA-HBED-CC PET (left) and (^{99}m)Tc-DPD BS (right) images in patient 9. In the PET/CT there is a bone metastasis (white arrow) in the lumbar spine which can be seen in the CT and PET, but not in the BS.

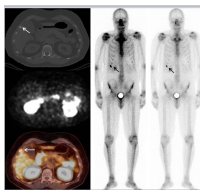

Figure 4: [^{68}Ga]Ga-PSMA-HBED-CC PET (left) and (^{99}m)Tc-DPD BS (right) images in patient 17. This is an example of a metastasis of Costa 8 right in the BS (black arrow) and in the CT (white arrow) which could not be detected in PET due to an intense signal of the liver.

Pat. No.	1st line therapy	2nd line therapy	3rd line therapy	PSA (ng/ml)	Therapy after
1	RRP[1], LNE[2], RTX[3]			0.7	Cyberknife for bone metastases
2	RRP, LNE	Salvage RTX	Bicalutamide*	1.2	none
3	AHT*			13.2	Zoledronic acid*
4	RRP, LNE			2.5	AHT[4]
5	Primarius			60	AHT, RTX
6	RRP, LNE, RTX			0.5	AHT
7	RRP, LNE	Bicalutamide		1.8	none
8	RRP, LNE			9.6	RTX for bone metastases
9	GnRH agonist*, Bicalutamide			n.a.	RTX for bone metastases
10	Primarius			45	RRP
11	RRP	Enzalutamide*		11.6	Alpharadin*
12	GnRH agonist*, Zoledronic acid			n.a.	none
13	RRP, LNE	RTX		3.5	AHT, RTX for bone metastases
14	RRP, Zoledronic acid			1.4	None
15	RRP, LNE			59.8	Cyberknife for bone metastases
16	RRP, LNE	Cetuximab*		3.4	none
17	RRP, LNE, Bicalutamide	RTX		9.5	none
18	RTX			8	none
19	RRP			2.5	AHT, Zoledronic acid

[1]radical retropubic prostatectomy; [2]lymphadenectomy; [3]radiotherapy; [4]anti-hormonal treatments. *Systemic regimens (e.g., chemotherapy, antihormone therapy, alpharadin therapy).

Table 1: Treatment histories of prostate cancer patients prior to imaging.

Discussion

Bone metastases are very common in patients with prostate cancer [10]. An autopsy study of men who died of prostate cancer suggests that bone metastases are present in up to 80% of cases [13]. The strong tendency of prostate cancer to spread to the skeletal system has been attributed to different mechanisms including reduced cell adhesion [14-16]. In addition, a complex tumor/microenvironment interaction appears to be involved. Many morphologic and metabolic imaging modalities have been studied for the detection of bone metastases in men with prostate cancer, but no consistent picture has emerged [17-20]. To our knowledge, this is the first study to provide data on the sensitivity, specificity, accuracy, and positive/negative predictive value of [^{68}Ga]Ga-PSMA-HBED-CC PET for the detection of bone metastases in prostate cancer.

Using CT and clinical parameters as standard of reference, our lesion-based analysis yielded 45.6% sensitivity, 86.4% specificity, 60.5% accuracy, 85.5% PPV and 47.7% NPV for [^{68}Ga]Ga-PSMA-HBED-CC PET. Our findings suggest that PET has significantly higher sensitivity than BS although (^{99}m)Tc-DPD BS is generally known for high sensitivity in the detection of bone metastases. The low sensitivity of 34% for the detection of bone metastases by BS in our study might be attributable to the deficiency of our standard of reference.

In general, ^{18}F-FDG PET is considered to be superior to (^{99}m)Tc-DPD BS in the detection of general bone metastases detection [21]. Nevertheless, the role of ^{18}F-FDG PET/CT in the detection of bone metastases from prostate cancer remains unclear and seems to be dependent on histology, tumor progression, morphology, and previous treatment of bone metastases [22]. Tumor progression and aggressiveness of prostate cancer defined by rising PSA levels result in a sensitivity rate of 77% for the detection of bone metastases by ^{18}F-FDG PET [23]. Sclerotic bone metastases are associated with less ^{18}F-FDG uptake than other morphological types of bone metastases [24]. Similar results have been reported for bone metastases from other primaries imaged by ^{18}F-choline PET/CT [20,25]. The reasons for reduced uptake appear to be different for ^{18}F-FDG and ^{18}F-choline [26]. Our results also suggest reduced tracer uptake kinetics in completely sclerotic bone metastases using the new radiotracer [^{68}Ga]Ga-PSMA-HBED-CC.

It has already been discussed in literature whether the detection rate is affected by functional and morphologic changes in bone metastases

following systemic treatment [22,25]. For instance, Fogelman and coworkers describe bone metastases becoming sclerotic after antihormonal therapy due to an intense osteoblastic healing process [24].

As shown in our study population, most prostate cancer bone metastases are of the osteoblastic to sclerotic morphologic type anyway. These lesions are difficult to differentiate from a treatment response of bone metastases. On CT scans-our imaging standard of reference-osteoblastic lesions can hardly be classified into active malignant lesions and regressive lesions with residual bone transformation. This problem is amplified for metabolic imaging as shown in the study of Israel et al. [27] using ^{18}F-FDG for the detection of bone metastases.

The limitations of CT as a standard of reference for treated bone metastases is certainly an important reason for the 49 false-negative bone metastases in [^{68}Ga]Ga-PSMA-HBED-CC PET. Another possible explanation is the fact that all metastases missed in our study by [^{68}Ga]Ga-PSMA-HBED-CC PET were small (<10 mm diameter) and completely sclerotic (670 HU to 1052 HU) in CT. Beheshti et al. [20] found that sclerotic bone metastases with attenuation above 825 HU measured by CT did not take up ^{18}F-choline. Ruf et al. [28] described another influence on tracer uptake kinetics in lesions: the maximum standard uptake value (SUV_{max}) was found to be distorted by partial volume effects (PVE) for lesions <21.4 mm in mathematical analysis and for lesions <25 mm in visual analysis. Hence, the dependence of lesion size to PVE seems to be much larger than assumed in the literature before (<15 mm) [29].

Limitations of this study are the retrospective study design, the small sample size, and the standard of reference. Nevertheless, the retrospective study design allowed us to obtain initial results with no additional radiation exposure or discomfort from additional examinations. Large sample sizes in future studies would be interesting to further stratify the influence of bone metastasis morphology on imaging by [^{68}Ga]-HBED-CC PSMA PET. As already mentioned, it is complicated to define an optimal standard of reference for bone metastases. All known imaging modalities are limited in the differentiation of treated bone metastases. A biopsy of all bone lesions with histopathological validation is ethically not feasible and not very practical. It would be a heavy interference into the patient's integrity. An optimal approach is currently not available. A partial solution would be the increased use of supplemental clinical parameters such as PSA to assess treatment response. Therefore, a reasonable amount of bone metastases should be monitored with PSA samples taken at regular intervals in a selected cohort of patients with clear PSA level to tumor burden correlation. The statistical results are reliable regarding the difference in sensitivities between both methods. Despite the small patient number there was enough statistical power for this result of the study. The exact values of sensitivity, specificity, PPV and NPV deriving from this study have to be considered very critically. For defining exact values the standard of reference is too weak and the patient number too small.

Despite these limitations, our study of a new promising radiotracer for the detection of bone metastases in prostate cancer has shown a clear benefit of [^{68}Ga]Ga-PSMA-HBED-CC PET. The new radiotracer clearly detected additional bone metastases in comparison to the current standard in nuclear medicine, (^{99}m)Tc-DPD BS. Further studies should evaluate the potential use in evaluating the response to systematic treatment. Therefore, the problem of the standard of reference of verifying bone metastases after systemic has to be solved in a practicable way.

Acknowledgement

V. Schreiter is participant in the Charité Clinical Scientist Program funded by the Charité Universitätsmedizin Berlin and the Berlin Institute of Health.

References

1. Oromieh AA, Avtzi E, Giesel FL, Letz HT, Linhart HG, et al. (2015) The diagnostic value of PET/CT imaging with the (68)Ga-labelled PSMA ligand HBED-CC in the diagnosis of recurrent prostate cancer. Eur J Nucl Med Mol imaging 42: 197-209.
2. Oromieh AA, Zechmann CM, Malcher A, Eder M, Eisenhut M, et al. (2014) Comparison of PET imaging with a (^{68})Ga-labelled PSMA ligand and (18)F-choline-based PET/CT for the diagnosis of recurrent prostate cancer. Eur J Nucl Med Mol imaging 41: 11-20.
3. Oromieh AA, Malcher A, Eder M, Eisenhut M, Linhart HG, et al. (2013) PET imaging with a [68Ga]gallium-labelled PSMA ligand for the diagnosis of prostate cancer: biodistribution in humans and first evaluation of tumour lesions. Eur J Nucl Med Mol imaging 40: 486-495.
4. Eder M, Neels O, Muller M, Bauder-Wust U, Remde Y, et al. (2014) Novel Preclinical and Radiopharmaceutical Aspects of [68Ga]Ga-PSMA-HBED-CC: A New PET Tracer for Imaging of Prostate Cancer. Pharmaceuticals 7: 779-796.
5. Silver DA, Pellicer I, Fair WR, Heston WD, Cordon-Cardo C, et al. (1997) Prostate-specific membrane antigen expression in normal and malignant human tissues. Clin Cancer Res 3: 81-85.
6. Hillier SM, Maresca KP, Femia FJ, Marquis JC, Foss CA, et al. (2009) Preclinical evaluation of novel glutamate-urea-lysine analogues that target prostate-specific membrane antigen as molecular imaging pharmaceuticals for prostate cancer. Cancer Res 69: 6932-6940.
7. Oromieh AA, Haberkorn U, Eder M, Eisenhut M, Zechmann CM, et al. (2012) [68Ga]Gallium-labelled PSMA ligand as superior PET tracer for the diagnosis of prostate cancer: comparison with 18F-FECH. Eur J Nucl Med Mol imaging 39: 1085-1086.
8. Jemal A, Siegel R, Xu J, Ward E (2010) Cancer statistics, 2010. CA Cancer J Clin 60: 277-300.
9. Siegel R, Naishadham D, Jemal A. (2012) Cancer statistics, 2012. CA Cancer J Clin 62: 10-29.
10. Jin JK, Dayyani F, Gallick GE (2011) Steps in prostate cancer progression that lead to bone metastasis. Int J Cancer 128: 2545-2561.
11. Sfoungaristos S, Frank SJ, Duvdevani M, Gofrit ON, Yutkin V, et al. (2014) Contemporary pharmacotherapy for the prevention of skeletal complications in patients with prostate cancer. Expert Opin Pharmacother 15: 2513-2514.
12. Langsteger W, Haim S, Knauer M, Waldenberger P, Emmanuel K, et al. (2012) Imaging of bone metastases in prostate cancer: an update. J Nucl Med Mol Imaging 56: 447-458.
13. Bubendorf L, Schopfer A, Wagner U, Sauter G, Moch H, et al. (2000) Metastatic patterns of prostate cancer: an autopsy study of 1,589 patients. Human pathol 31: 578-583.
14. Mol AJ, Geldof AA, Meijer GA, van der Poel HG, van Moorselaar RJ, et al. (2007) New experimental markers for early detection of high-risk prostate cancer: role of cell-cell adhesion and cell migration. J Cancer Res Clin Oncol 133: 687-695.
15. Bussemakers MJ, van Moorselaar RJ, Giroldi LA, Ichikawa T, Isaacs JT, et al. (1992) Decreased expression of E-cadherin in the progression of rat prostatic cancer. Cancer Res 52: 2916-2922.
16. Tremblay L, Hauck W, Aprikian AG, Begin LR, Chapdelaine A, et al. (1996) Focal adhesion kinase (pp125FAK) expression, activation and association with paxillin and p50CSK in human metastatic prostate carcinoma. Int J Cancer 68: 164-171.

17. Shen G, Deng H, Hu S, Jia Z (2014) Comparison of choline-PET/CT, MRI, SPECT, and bone scintigraphy in the diagnosis of bone metastases in patients with prostate cancer: a meta-analysis. Skeletal Radiol 43: 1503-1513.
18. Yang HL, Liu T, Wang XM, Xu Y, Deng SM, et al. (2011) Diagnosis of bone metastases: a meta-analysis comparing (1)(8)FDG PET, CT, MRI and bone scintigraphy. Eur Radiol 21: 2604-2617.
19. Balogova S, Zakoun JB, Michaud L, Khalil A, Tassart M, et al. (2014) Whole-body 18F-fluorocholine (FCH) PET/CT and MRI of the spine for monitoring patients with castration-resistant prostate cancer metastatic to bone: a pilot study. Clin Nucl Med 39: 951-959.
20. Beheshti M, Vali R, Waldenberger P, Fitz F, Nader M, et al. (2009) The use of F-18 choline PET in the assessment of bone metastases in prostate cancer: correlation with morphological changes on CT. Mol Imaging Biol 11: 446-454.
21. Schirrmeister H, Guhlmann A, Elsner K, Kotzerke J, Glatting G, et al. (1999) Sensitivity in detecting osseous lesions depends on anatomic localization: planar bone scintigraphy versus 18F PET. J Nucl Med 40: 1623-1629.
22. Fogelman I, Cook G, Israel O, Van der Wall H (2005) Positron emission tomography and bone metastases. Semin Nucl Med 35: 135-142.
23. Morris MJ, Akhurst T, Osman I, Nunez R, Macapinlac H, et al. (2002) Fluorinated deoxyglucose positron emission tomography imaging in progressive metastatic prostate cancer. Urology 59: 913-918.
24. Shreve PD, Grossman HB, Gross MD, Wahl RL (1996) Metastatic prostate cancer: initial findings of PET with 2-deoxy-2-[F-18]fluoro-D-glucose. Radiology 199: 751-756.
25. Cook GJ, Houston S, Rubens R, Maisey MN, Fogelman I, et al. (1998) Detection of bone metastases in breast cancer by 18FDG PET: differing metabolic activity in osteoblastic and osteolytic lesions. J Clin Oncol 16: 3375-3379.
26. Reske SN, Blumstein NM, Neumaier B, Gottfried HW, Finsterbusch F, et al. (2006) Imaging prostate cancer with 11C-choline PET/CT. J Nucl Med 47: 1249-1254.
27. Israel O, Goldberg A, Nachtigal A, Militianu D, Bar-Shalom R, et al. (2006) FDG-PET and CT patterns of bone metastases and their relationship to previously administered anti-cancer therapy. Eur J Nucl Med Mol Imaging 33: 1280-1284.
28. Ruf J, Schiefer J, Kropf S, Furth C, Ulrich G, et al. (2013) Quantification in Ga-DOTA(0)-Phe(1)-Tyr(3)-octreotide positron emission tomography/computed tomography: can we be impartial about partial volume effects? Neuroendocrinology 97: 369-374.
29. Wieder H, Beer AJ, Poethko T, Meisetschlaeger G, Wester HJ, et al. (2008) PET/CT with Gluc-Lys-([(18)F]FP)-TOCA: correlation between uptake, size and arterial perfusion in somatostatin receptor positive lesions. Eur J Nucl Med Mol Imaging 35: 264-271.